Spectroscopic analysis of up conversion luminescence in doped halogeno-antimonite glass

M. Iezid, F. Goumeidane, A. Abidi, N. Gherraf, M. Legouera, M. Poulain, T. Satyanarayana, P.S. Prasad, P.V. Rao

Spectroscopic analysis of up conversion luminescence in doped halogeno-antimonite glass

M.Iezid[1], F.Goumeidane[2], A.Abidi[3], N.Gherraf[4], M.Legouera[5], M.Poulain[6], T. Satyanarayana[7], P. Syam Prasad[8], P.Venkateswara Rao[*]

[1]Laboratoire d'Innovation en construction, Eco-conception et Génie Sismique (LICEGS) ; Université Mostafa Ben Boulaid Batna 2 (Algeria)

[2]Laboratory of Active Components and Materials; Larbi Ben M'hidi University,Oum El Bouaghi, 04000, (Algeria).

[3]Département Génie des procédés ; Université Annaba (Algérie)
[4]Laboratoire des Ressources Naturelles et Aménagement des Milieux Sensibles ; Larbi Ben M'hidi University,Oum El Bouaghi, 04000, (Algeria).

[5]Laboratoire de Génie Mécanique et Matériaux ; Université 20 Aout 1955 Skikda (Algeria)

[6]Institut des Sciences Chimiques de Rennes, Université Rennes 1 (France).
[7]Dept. of Electronics & Instrumentation Engineering, Lakireddy Bali Reddy College of Engineering (A), Mylavaram, Krishna 521230, A.P., India

[8]Dept. of Physics, National Institute of Technology (NIT), Warangal-506 004, Telangana State, India

[*] Department of Physics, The University of the West Indies, Mona Campus, Jamaica

* Corresponding author : pvrao54@gmail.com (P. Venkateswara Rao)

Abstract

The up-conversion emission of Nd^{3+}, Sm^{3+} and Er^{3+} has been studied in a new halogeno-antimonite glass with the chemical composition 80 Sb_2O_3 - 10 $ZnBr_2$ - 10 KCl. Doping concentration was 0.2 mol% of lanthanide (Ln) ions. Rare earths were introduced as fluorides LnF_3 that were further converted into oxides. Main physical properties of base glass were measured, including density, thermal expansion, characteristic temperatures, refractive index and optical transmission. The amount of residual hydroxyls was calculated from the OH absorption band around 3000 nm. The recorded up-conversion emission lines are λ_{em} = 536 nm for Nd^{3+} pumped at 805 nm; λ_{em} = 563 nm, 600 nm, 631 nm and 645 nm for Sm^{3+} pumped at 945 nm; λ_{em} = 531 nm for Er^{3+} pumped at 798 nm. Co-doped glass (0.1 Yb^{3+} + 0.1 Er^{3+}) pumped at 980 nm has three emission lines at 524 nm, 545 nm and 650 nm. Corresponding transitions have been identified and the mechanisms ruling the up-conversion process is discussed. They include excited state absorption (ESA), energy transfer (ET) cooperative energy transfer (CET), emission assisted by phonon (EAP), multiphonon relaxation (MR) and cross- relaxation (CR).

Key words: Melt-quenching; doped glass; low phonon energy; HMOGs Glasses; Up-Conversion Luminescence

1. Introduction:

The conversion of infrared radiation into visible light has attracted much attention for the last twenty five years, especially in lanthanide doped fluoride glasses [1-17]. It leads to a large number of new laser lines, especially in fiber lasers [18]. Potential technological applications include color display, sensors, optical data storage, biomedical diagnostics, and undersea communications [19-22]. Physically the infrared to visible conversion may be described as an anti-Stokes emission. While it was first discovered by N. Bloembergen [23], most important contributions rose from the papers of F. Auzel [24]. This process is based on the absorption of one or two photons from an already excited state absorption (ESA), called metastable intermediate level. The emissive levels are populated either directly or with phonon assistance [24]. Optical pumping occurs from the ground state, using broadband sources (e.g. xenon lamp) or laser diodes. As a result, red, green or blue light can be emitted.

Trivalent lanthanides used for up-conversion are: Nd^{3+}, Sm^{3+}, Er^{3+}, Tm^{3+}, $Tb^{3+}$and Ho^{3+}. Classically, Yb^{3+} is often added as a co-dopant to maximize energy transfer [1, 18, 24]. The solid state matrix must have the low phonon energy and optimized lanthanide concentration to have a good conversion efficiency. Major groups of up-conversion glasses include heavy metal fluoride glasses, especially ZBLAN [25-27], chalcogenide glasses [28], and heavy metal oxide glasses (HMOGs) [29-32]. This latter family of glasses is characterized by a low phonon energy ($700\ cm^{-1} \leq E_p < 800\ cm^{-1}$), a good chemical durability, especially in liquid water and mechanical properties. Up-conversion has been studied in multicomponent glasses based on the oxides of Te , Ge , Bi and Pb as major components stabilized by oxides of Zn , Ga , W and Nb [33-36].

Sb_2O_3 contributes in the glass network with SbO_3 structural units and it appears tetrahedra with the oxygens to be found at three corners and the lone pair of electrons of antimony Sb^{3+} at the fourth corner localized in the third equatorial direction of the Sb atom. There may be a possibility of existence of antimony ions in the Sb^{5+} state and participate in the glass network forming with $Sb^{5+}O_4$ structural units may enhance the nonlinear optical properties [48].Antimonite glasses are based on Sb_2O_3 as a glass former. They belong to the group of HMOG and have been reported in a large number of vitreous systems [37-46]. They exhibit large linear and non-linear refractive index. Some work was devoted to the study of the

infrared to visible conversion in antimonite based glassy matrices. Their phonon energy is ruled by the vibration of the Sb - O bond, which is nearly 600 cm^{-1} [46].

Our work is centered upon the study of the up-conversion emission in a new antimonite glass with the chemical composition 80 Sb_2O_3 – 10 $ZnBr_2$ – 10 KCl. It has been doped with Nd, Sm, Er, and Yb/Er. We report the general physical properties of this glass. They include density, characteristic temperatures, thermal expansion, optical transmission and refractive index. Recorded emission spectra are discussed on the basis of the well-known energy diagrams of trivalent lanthanides, and the mechanisms involved in the up-conversion process.

2. Experimental

Glass synthesis was made by the standard melt/quenching method, at around 650 °C in a silica tube. Samples were annealed in the vicinity of the glass transition temperature Tg. The chemicals used were: $Sb_2O_3 \geq 99\%$ (Across), $ZnBr_2 > 99\%$ (Merck)), KCl ≈ 99 % (Fluka), LnF_3 ≈ 99.9 % (Alfa Aesar) {Ln = Nd ; Sm ; Er ; Yb}. Base glass composition was 80 Sb_2O_3 – 10 $ZnBr_2$ – 10 KCl. Doped glasses comply with the following compositions: 80 Sb_2O_3 – 9.8 $ZnBr_2$ – 10 KCl – 0.2 LnF_3 {Ln = Nd ; Sm ; Er}. The co-doped glass comprises: 80 Sb_2O_3 – 9.8 $ZnBr_2$ – 10 KCl – 0.1 YbF_3 – 0.1 ErF_3. Lanthanide fluorides were chosen as starting materials because they lead to more homogeneous samples than those obtained with oxides. However, it must be outlined that final samples do not contain anymore fluorine as silica is used as material crucible. In the synthesis process, fluorine is replaced by oxygen according to the chemical reaction:

$$4\ LnF_3 + 3\ SiO_2 \rightarrow 2\ Ln_2O_3 + 3\ SiF_4$$

Density was measured using helium pycnometer ACCUPYC 1330 (Micromeritics). Differential Scanning Calorimetry was implemented between 20 °C and 500 °C, using a DSC Q20 model from TA instruments, with a 10 K / min heating rate and a 0.1 K sensitivity. The thermal expansion was measured at 4 K heating rate, using a thermo-mechanical analyzer TMA 2940 from TA instruments. Optical transmission in the UV-visible range was recorded between 350 and 800 nm by a Perkin Elmer spectrophotometer. Infrared absorption was measured between 400 and 4000 cm^{-1} using a TENSOR 37 FTIR infrared spectrophotometer. The UV-Vis cut-off is taken at a threshold of 40 % of transmission, while the limit of IR transparency λ_{MP} corresponds to 0 % transmission. The refractive index was measured by Olympus BX 60 type optical microscope according to the method known as " the apparent

depth " [37, 47]. The accuracy in the index value is 10^{-2} if both sides are parallel and carefully polished. The thickness of the samples intended for the optical measurements is about 3 mm.

The emission spectra of doped glasses were made using a spectrofluorometer model "Fluorolog FL3 -22 Jobin- Yvon - SPEX" at room temperature. Optical excitation is achieved by a xenon arc lamp of 450 Watts, emitting a polychromatic radiation between 200 and 900 nm. The double excitation monochromator comprises two networks of 1200 lines per mm, jaded at 250 nm. The emission one has the same number of strokes but they are jaded at 500 nm. This configuration allows the first double monochromator to have a great rejection of the stray white light. The optimal sensitivity of the second one lies in the 300-850 nm range. The samples are placed in vats inclined 22.5° with respect to the incident light to avoid interference between the excitation light and up-conversion signal.

3. Results:

Our results fall into two categories: the first focuses on the physical characteristics of the new glassy matrix (80 Sb_2O_3 – 10 $ZnBr_2$ – 10 KCl), and the second shows the up-conversion emission of the matrix doped with trivalent lanthanides and the same spectrum of the Yb:Er co-doped glass.

3.1. Physical properties of the80 Sb_2O_3 –10 $ZnBr_2$ –10 KCl glass

Figure 1 shows the DSC curve of the antimonite glass 80 Sb_2O_3 – 10 $ZnBr_2$ – 10 KCl where it clearly shows the glass transition and the crystallization peak (exothermic). Figure (2.a, b) shows the curves of UV-visible and infrared optical transmission. From these we determine transmission thresholds. Extrinsic absorption bands appear in the infrared curve due to contamination of silica tube (1^{st} overtone of the Si-O vibration), gaseous CO_2 in spectrometer, and finally, moisture (OH band). The OH amount (in ppm) can be calculated according to the procedure reported in the literature [46], $Q=30.\alpha$ (α absorption coefficient at 3323 cm^{-1}).

Main physical properties of this glass are gathered at tables 1a and 1b.They are close to those reported for other antimonite glasses [37-46].

3.2. Up- conversion emission:

Figures 3, 4, 5 and 6 show the emission spectra of doped and co-doped glasses. The Nd^{3+} ions emit green light at 536 nm under 805 nm infrared excitation, which corresponds to the $^4G_{7/2}$

$\rightarrow {}^4I_{9/2}$ transition (fig.3). In the case of Sm^{3+}, four upconversion emission lines are observed, corresponding to the ${}^4G_{5/2} \rightarrow {}^6H_J$ (J=5/2 ; 7/2 ; 9/2 ; 11/2) transitions. The corresponding wavelengths are respectively: 536 nm, 600 nm, 631 nm, 645 nm and excitation wavelength is 949 nm (Fig.4).

The Er^{3+} doped glass emits green light at 531 nm under 798 nm excitation. It corresponds to the ${}^4S_{3/2} \rightarrow {}^4I_{15/2}$ transition (fig.5). The (Yb^{3+}, Er^{3+}) co-doped glass has two green emission lines at 524 nm and 545 nm, and also a red emission line at 650 nm. Infrared excitation is implemented at 980 nm and the active transitions are:

${}^2H_{11/2} \rightarrow {}^4I_{15/2}$; ${}^4S_{3/2} \rightarrow {}^4I_{15/2}$; ${}^4F_{9/2} \rightarrow {}^4I_{15/2}$.

The Yb^{3+} / Er^{3+} co-doping results in the population of two additional levels ${}^2H_{11/2}$ and ${}^4F_{9/2}$ and two additional emission lines, by comparison to the glass doped only with Er^{3+}. It also further increases the population of the ${}^4S_{3/2}$ level, which is exemplified by the respective intensities: 6916 CPS vs 9257 CPS for co- doped sample (Fig. 5 and 6).

The up-conversion emissions, thus harvested are close to those of the KBS antimonite glass doped with Nd^{3+}, Sm^{3+} and Er^{3+} cations [46].

4. Discussion:

The up- conversion process of Nd^{3+} in this glass is described in the energy diagram of figure 7. In a first step an electron of the ground state ${}^4I_{9/2}$ is promoted to the excited state ${}^4F_{5/2}$ (GSA) by a photon at 805 nm. Then a non- radiative relaxation occurs between the two levels ${}^4F_{5/2}$ and ${}^4F_{3/2}$.

In a second step, the 805 nm pump move an electron from the excited metastable level ${}^4F_{3/2}$ to the higher excited state ${}^2D_{5/2}$. This process corresponds to excited state absorption (ESA) which may be described as follows:

${}^4I_{9/2} \rightarrow {}^4F_{5/2}$ (GSA) $\rightarrow {}^4F_{3/2}$ (NR) $\rightarrow {}^2D_{5/2}$ (ESA).

It is followed by a multiphonon relaxation between the upper level ${}^2D_{5/2}$ and the emission level ${}^4G_{7/2}$. This gives rises to a green emission at 536 nm corresponding to the transition between the emissive level ${}^4G_{7/2}$ and the ground state ${}^4I_{9/2}$. The two-photon excitation mode described above, is dominant in at low Nd^{3+} concentration.

Increasing Nd^{3+} concentration reduces the distance between rare earth ions. This enhances energy exchange between neighboring Nd^{3+}. This exchange is of two types:

The first one is called “energy transfer” (ET). It occurs between two Nd^{3+} neighbors and led to populate the emission level $^4G_{7/2}$. In this case two excited Nd^{3+} ions at intermediary state exchange excitation according to the following resonant scheme: ($^4F_{3/2}$, $^4F_{3/2}$) → ($^4I_{13/2}$, $^4G_{7/2}$). As a result, one Nd^{3+} reaches to the excited state $^4G_{7/2}$while the other one relaxes to the ground state. Another (ET) possibility is ($^4F_{3/2}$, $^4F_{3/2}$) → ($^4I_{11/2}$, $^2G_{9/2}$) [35] : ($^4F_{3/2}$, $^4F_{3/2}$) → ($^4I_{11/2}$, $^2G_{9/2}$) ; so, after transfer, a Nd^{3+} ion jumps to the higher excited state $^2G_{9/2}$ while the other one returns to ground state $^4I_{9/2}$. This type of energy transfer increases the population of the emission level $^4G_{7/2}$. It is efficient in low phonon energy matrices such as antimonites.

A second type of energy exchange between Nd^{3+} ions is likely to occur. It depopulates emissive level $^4G_{7/2}$ (or $^2G_{7/2}$ since this level is in thermal equilibrium with $^4G_{7/2}$). This process is called cross-relaxation (CR) where the possible resonant channels are:

($^4G_{7/2}$, $^4I_{9/2}$) → ($^4F_{7/2}$, $^4I_{15/2}$) and ($^2G_{7/2}$, $^4I_{9/2}$) → ($^4F_{3/2}$, $^4I_{15/2}$).

The up-conversion mechanism of Sm^{3+} in antimonite glass is shown in figure 8. The first absorption of the pump at 949 nm corresponds to the $^6H_{5/2} \rightarrow {}^6F_{11/2}$ transition (GSA) while the absorption of the second photon follows different paths: either ESA according to $^6F_{11/2} \rightarrow {}^4I_{11/2}$ or, after non radiative transitions $^6F_{11/2} \rightarrow {}^6F_{9/2}$ (NR) or $^6F_{11/2} \rightarrow {}^6F_{7/2}$ (NR), the second photon is absorbed as follows:

$^6H_{5/2} \rightarrow {}^6F_{11/2}$ (GSA) → $^6F_{9/2}$ (NR) → $^4G_{7/2}$ (ESA) or $^6H_{5/2} \rightarrow {}^6F_{11/2}$ (GSA) → $^6F_{7/2}$ (NR) → $^4F_{3/2}$ (ESA).

In all cases, multiphonon relaxation from the final levels of the higher excited state (ESA) leads to populating the emissive level $^4G_{5/2}$. Finally the emission of four colors occurs:

$^4G_{5/2} \rightarrow {}^6H_J$ (J = 11/2; 9/2; 7/2 ; 5/2)

Energy transfer is likely to populate the emissive level according to following schemes:

($^6F_{11/2}$, $^6F_{11/2}$) → {($^6H_{5/2}$, $^4I_{11/2}$); ($^6H_{7/2}$, $^4I_{9/2}$); ($^6H_{9/2}$, $^4F_{3/2}$); ($^6H_{11/2}$, $^4G_{5/2}$)}.

On the another side the red emission towards 631 nm can be improved by cooperative transfer of energy (CET), involving two Sm^{3+} excited at levels $^4I_{9/2}$ and $^6F_{7/2}$ by one resonant cross relaxation (RCR) of type $^4I_{9/2} \rightarrow {}^4G_{5/2}$ et $^6F_{7/2} \rightarrow {}^6F_{11/2}$; this also contributes to populating the $^4G_{5/2}$ emissive level. This type of transfer is favorable if the shift between the two gaps of the preceding transitions is about 100 cm^{-1}. As previously mentioned this category of transition takes place only if the distance between Sm^{3+} cations is satisfactory.

Note that cross relaxation depopulates the $^4G_{5/2}$ level according to: ($^4G_{5/2}$, $^6H_{5/2}$) → 2 $^6F_{9/2}$.

Infrared to visible conversion observed in the Er^{3+} doped antimonite glass is explained in the energy diagram of figure 9 that denotes a green emission (λ_{em}= 531 nm). Pump wavelength was close to 798 nm. The following sequence of transitions leads to this emission:

Excitation: $^4I_{15/2} \rightarrow {}^4I_{9/2}$ (GSA) $\rightarrow$ **{**$^4I_{11/2}$ (NR) $\rightarrow {}^4F_{3/2}$ (ESA) or $^4I_{13/2}$ (NR) $\rightarrow {}^4F_{7/2}$ (ESA)**}** ;

Nonradiative transition: $^4F_{3/2}$ (ESA) $\rightarrow {}^4S_{3/2}$ (NR) and $^4F_{7/2}$ (ESA) $\rightarrow {}^4S_{3/2}$ (NR), knowing that $^4S_{3/2}$ and $^2H_{11/2}$ are in thermal equilibrium.

Emission: $^4S_{3/2} \rightarrow {}^4I_{15/2}$ (U.C).

The energy transfers are: ($^4I_{11/2}$, $^4I_{11/2}$) $\rightarrow$ ($^4I_{15/2}$, $^4F_{7/2}$) (ET) et ($^4I_{11/2}$, $^4I_{9/2}$) $\rightarrow$ ($^4I_{15/2}$, $^4F_{5/2}$) (ET)

Cross relaxations are done by: ($^4F_{7/2}$, $^4I_{15/2}$) $\rightarrow$ (2 $^4I_{11/2}$) (CR) et ($^4S_{3/2}$, $^4I_{15/2}$) $\rightarrow$ ($^4I_{9/2}$,$^4I_{13/2}$) (CR).

In the case of the (Yb^{3+}; Er^{3+}) co-doped glass, pump wavelength is 980 nm and the corresponding energy diagram accounting for up-conversion is represented in figure 10. Ytterbium acts as sensitizer and Erbium as activator. The 980 nm excitation leads to the transition:

Yb^{3+}: $^2F_{7/2} \rightarrow {}^2F_{5/2}$.

The first stage corresponds to energy transfer from Yb^{3+} to Er^{3+} according to:

$^2F_{5/2}$ (Yb^{3+}) + $^4I_{15/2}$ (Er^{3+}) $\rightarrow$ $^4I_{11/2}$ (Er^{3+}) + $^2F_{7/2}$ (Yb^{3+}).

A second photon could be absorbed by Er^{3+} starting from the metastable level $^4I_{11/2}$ (Er^{3+}) ; where the exchange between Yb^{3+}/Er^{3+} is summarized as follows: $^2F_{5/2}$ (Yb^{3+}) + $^4I_{11/2}$ (Er^{3+}) $\rightarrow$ $^2F_{7/2}$ (Yb^{3+}) + $^4F_{7/2}$ (Er^{3+} : ESA).

The energy shift is limited between the higher excited level $^4F_{7/2}$ (Er^{3+}) and levels $^2H_{11/2}$ (Er^{3+}) and $^4S_{3/2}$ (Er^{3+}). Then, following the multiphonon relaxation the Er^{3+} ion emits two green lines at 524 nm and 545 nm. These two emissions are the result of an up-conversion process that may be expressed by:

Er^{3+}: $^4F_{7/2} \rightarrow {}^2H_{11/2}$ (NR) $\rightarrow {}^4I_{15/2}$ (UC): 524 nm.

Er^{3+}: $^4F_{7/2} \rightarrow {}^4S_{3/2}$ (NR) $\rightarrow {}^4I_{15/2}$ (UC): 545 nm.

The second line is very close to the primary green selected by CIE as reference (546.1 nm). It corresponds to the mercury emission.

The up-conversion emission of the average red (λ_{em}= 650 nm), results from the transition Er^{3+}: $^4F_{9/2} \rightarrow {}^4I_{15/2}$ (UC). As outlined above, the exchange between Yb^{3+}/Er^{3+} populates the $^4I_{11/2}$ level of Er^{3+} according to: $^2F_{5/2}$ (Yb^{3+}) + $^4I_{15/2}$ (Er^{3+}) → $^4I_{11/2}$ (Er^{3+}) + $^2F_{7/2}$ (Yb^{3+}).

The 650 nm up-conversion emission is explained through the following sequence:

Er^{3+}: $^4I_{11/2}$ (GSA) → $^4I_{13/2}$ (NR) → $^4F_{9/2}$ (ESA) → $^4I_{15/2}$ (UC).

Two channels of cross relaxation are probable:

Er^{3+}: ($^4I_{11/2}$, $^4I_{11/2}$) → ($^4I_{15/2}$, $^4F_{7/2}$) (CR)

Er^{3+}: ($^4I_{13/2}$, $^4I_{11/2}$) → ($^4I_{15/2}$, $^4F_{9/2}$) (CR)

These two channels depopulate the two emissive levels $^4F_{7/2}$ and $^4F_{9/2}$.

The halogenated compounds, namely zinc bromide $ZnBr_2$, reduce the phonon energy. In this respect, the phonon energy must take an intermediate value between the purely oxides glasses and the purely halogenated glasses [49]. In some cases the incorporation of a halide makes it possible to control the density of phonons. The up-conversion efficiency depends on intrinsic and extrinsic parameters. The weak phonon energy (≈ 600 Cm^{-1}) of the 80 Sb_2O_3 – 10 $ZnBr_2$ – 10 KCl vitreous matrix decreases notably the nonradiative transitions and enhances up-conversion emission. This feature is almost non-existent in classical glasses (borates, phosphates and silicates). In the same way the high value of the refraction index (1.97) increases the probability of the radiative transitions. Finally the broad transparency range that extends from 0.41 µm to 7.85 µm allows the antimonite matrix to transmit a wide range of colors.

The capacity of these antimonite glasses to accommodate trivalent lanthanides is limited, by comparison to other glasses such as phosphates and ZBLAN. Beyond 0.3 % molar of lanthanides, antimonite glasses free of classical formers (B_2O_3; P_2O_5) reach the solubility limit of trivalent lanthanides and start devitrifying.

Impurities, and namely and OH^- groups often act as quenchers. They are extrinsic elements of the glass. Hydoxyle OH^- exhibits a high vibration energy (≈ 3000 Cm^{-1}), which can bridge the energy gap between the $^4F_{9/2}$ and $^4I_{9/2}$ levels of the Er^{3+} ion. In the same way, two vibrational quanta of ion OH^- can bridge the gap between $^4I_{13/2}$ and $^4I_{15/2}$ of the ion Er^{3+}. A smaller quenching effect could arise from silicate traces.

While silica contamination may be avoided using convenient crucibles, hydroxyl concentration may be drastically reduced using optimized processing. This includes purification of starting materials, dry working atmosphere and incorporation of halides in the batch. In glass melt the following chemical reaction is expected to occur:

$F^- + OH^- \rightarrow HF\nearrow + O^{2-}$.

5. Conclusion:

A new antimonite glass with the chemical composition 80 Sb_2O_3 – 10 $ZnBr_2$ – 10 KCl has been investigated. It belong to the HMOG groups and has the following characteristics:

A good thermal stability ($T_x - T_g$ = 109 °C)

A low phonon energy ($E_p \approx 600$ cm^{-1})

A high refraction index (n = 1.97)

A broad field of transparency (0.41 µm - 7.85 µm)

These features are favourable to Up-conversion emission after doping by various trivalent lanthanides (Nd^{3+}; Sm^{3+}; Er^{3+}; Yb^{3+} / Er^{3+}). We have recorded several up-conversion emissions at ambient temperature with a content of 0.2 mol % of lanthanides according to:

- **Nd^{3+}**: $^4G_{7/2} \rightarrow {}^4I_{9/2}$ with λ_{em}= 536 nm under 805 nm excitation;

- **Sm^{3+}**: $^4G_{5/2} \rightarrow {}^6H_J$ (J= 5/2; 7/2; 9/2; 11/2) where the wavelengths are respectively: 563 nm; 600 nm; 631 nm and 645 nm. Pump wavelength 949 nm.

- **Er^{3+}**: $^4S_{3/2} \rightarrow {}^4I_{15/2}$ with λ_{em}= 531 nm under 798 nm excitation.
- **Yb^{3+}/Er^{3+}** : $^2H_{11/2} \rightarrow {}^4I_{15/2}$; $^4S_{3/2} \rightarrow {}^4I_{15/2}$ et $^4F_{9/2} \rightarrow {}^4I_{15/2}$ correspondents respectively with the wavelengths 524 nm ; 545 nm et 650 nm. The excitation was made under 980 nm.

Several mechanisms rule these emissions namely: excited state absorption (ESA), energy transfer of (ET), cooperative transfer of energy (CET), multiphonon relaxation (MPR) and cross relaxation (CR).

The emission at 545 nm in the Yb^{3+}/Er^{3+} co-doped case is very close to the primary green to the mercury emission (546.1 nm). The latter is retained by the international commission of lighting (CIE) as reference.

References

[1] R. Quimby, M. Drexhage, M. Suscavage, Efficient frequency up-conversion via energy transfer in fluoride glasses, Electronics Letters, 23 (1987) 32-34.
[2] J. Allain, M. Monerie, H. Poignant, Room temperature CW tunable green upconversion holmium fibre laser, Electronics Letters, 26 (1990) 261-263.
[3] R. Smart, D. Hanna, A. Tropper, S. Davey, S. Carter, D. Szebesta, CW room temperature upconversion lasing at blue, green and red wavelengths in infrared-pumped Pr/sup 3+/-doped fluoride fibre, Electronics Letters, 27 (1991) 1307-1309.
[4] S. Grubb, K. Bennett, R. Cannon, W. Humer, CW room-temperature blue upconversion fibre laser, Electronics Letters, 28 (1992) 1243-1244.
[5] A.C. Tropper, J.N. Carter, R. Lauder, D.C. Hanna, S.T. Davey, D. Szebesta, Analysis of blue and red laser performance of the infrared-pumped praseodymium-doped fluoride fiber laser, JOSA B, 11 (1994) 886-893.
[6] S. Sanders, R. Waarts, D.G. Mehuys, D. Welch, Laser diode pumped 106 mW blue upconversion fiber laser, Applied physics letters, 67 (1995) 1815-1817.
[7] A. Saïssy, B. Dussardier, G. Maze, G. Monnom, S. Wade, Blue upconversion emission in Er^{3+}-doped fluoride fiber, Optical Fiber Technology, 2 (1996) 249-252.
[8] D.M. Baney, G. Rankin, K.-W. Chang, Blue Pr^{3+}-doped ZBLAN fiber upconversion laser, Optics letters, 21 (1996) 1372-1374.
[9] R. Paschotta, N. Moore, W.A. Clarkson, A.C. Tropper, D.C. Hanna, G. Mazé, 230 mW of blue light from a thulium-doped upconversion fiber laser, IEEE Journal of Selected Topics in Quantum Electronics, 3 (1997) 1100-1102.
[10] D. Funk, J. Eden, J. Osinski, B. Lu, Green, holmium-doped upconversion fibre laser pumped by red semiconductor laser, Electronics Letters, 33 (1997) 1958-1960.
[11] T. Sandrock, H. Scheife, E. Heumann, G. Huber, High-power continuous-wave upconversion fiber laser at room temperature, Optics letters, 22 (1997) 808-810.
[12] H. Zellmer, P. Riedel, M. Kempe, A. Tunnermann, High-power diode pumped upconversion fibre laser in red and green spectral range, Electronics Letters, 38 (2002) 1250-1251.
[13] G. Qin, S. Huang, Y. Feng, A. Shirakawa, M. Musha, K.-I. Ueda, Power scaling of Tm^{3+} doped ZBLAN blue upconversion fiber lasers: modeling and experiments, Applied Physics B, 82 (2006) 65-70.
[14] A.-H. Li, Q. Lü, Z.-R. Zheng, L. Sun, W.-Z. Wu, W.-L. Liu, H.-Z. Chen, Y.-Q. Yang, T.-Q. Lü, Enhanced green upconversion emission of Er^{3+} through energy transfer by Dy^{3+} under 800 nm femtosecond-laser excitation, Optics letters, 33 (2008) 693-695.
[15] O. Hellmig, S. Salewski, A. Stark, J. Schwenke, P.E. Toschek, K. Sengstock, V.M. Baev, Multicolor diode-pumped upconversion fiber laser, Optics letters, 35 (2010) 2263-2265.
[16] M. Hayakawa, T. Hayakawa, X.T. Zhang, M. Nogami, Optical detection of near infrared femtosecond laser-heating of Er^{3+}-doped $ZnO–Nb_2O_5–TeO_2$ glass by green up-conversion fluorescence of Er^{3+} ions, Journal of Luminescence, 131 (2011) 843-849.

[17] J. Méndez-Ramos, P. Acosta-Mora, J. Ruiz-Morales, T. Hernández, M. Borges, P. Esparza, Heavy rare-earth-doped ZBLAN glasses for UV–blue up-conversion and white light generation, Journal of Luminescence, 143 (2013) 479-483.
[18] M.J. Weber, Handbook of lasers, CRC press2000.
[19] Q. Jianbei, S. Zhiguo, Nanocrystals precipitation and up-conversion luminescence in Yb^{3+}-Tm^{3+} co-doped oxyfluoride glasses, Journal of rare earths, 26 (2008) 919-923.
[20] T. Hayakawa, M. Hayakawa, M. Nogami, Estimation of the fs laser spot temperature inside TeO_2–ZnO–Nb_2O_5 glass by using up-conversion green fluorescence of Er^{3+} ions, Journal of Alloys and Compounds, 451 (2008) 77-80.
[21] M. Ajroud, M. Haouari, H.B. Ouada, H. Mâaref, A. Brenier, B. Champagnon, Energy transfer processes in (Er^{3+}–Yb^{3+})-codoped germanate glasses for mid-infrared and up-conversion applications, Materials Science and Engineering: C, 26 (2006) 523-529.
[22] B. Peng, L. Jiang, X. Qiu, Z. Fan, W. Huang, Ytterbium doped heavy metal oxide glasses with high emission cross-section, Journal of alloys and compounds, 398 (2005) 170-172.
[23] N. Bloembergen, Solid state infrared quantum counters, Physical Review Letters, 2 (1959) 84.
[24] F. Auzel, Compteur quantique par transfert d'energie entre deux ions de terres rares dans un tungstate mixte et dans un verre, CR Acad. Sci. Paris, 262 (1966) 1016-1019.
[25] M. Poulain, M. Poulain, J. Lucas, Verres fluores au tetrafluorure de zirconium proprietes optiques d'un verre dope au Nd^{3+}, Materials Research Bulletin, 10 (1975) 243-246.
[26] A. Lecoq, M. Poulain, Phenomenological Study of the Stabilizing Role of Aluminum in Zirconium Tetrafluoride Glasses, Verres Refract, 34 (1980) 333-342.
[27] M. Poulain, Fluoride Glasses: properties, technology and applications, (2010).
[28] J.-L. Adam, X. Zhang, Chalcogenide glasses: preparation, properties and applications, Woodhead publishing2014.
[29] W.H. Dumbaugh, Lead bismuthate glasses, Physics and Chemistry of Glasses, 19 (1978) 121-125.
[30] J. Lapp, W.H. Dumbaugh, M. Powley, Heavy Metal Oxide Glasses, Riv. del Staz. Sper. Vetro, 1 (1989) 91-96.
[31] B. Zhou, C.F. Rapp, J.K. Driver, M.J. Myers, J.D. Myers, J. Goldstein, R. Utano, S. Gupta, Development of tellurium oxide and lead-bismuth oxide glasses for mid-wave infra-red transmission optics, Oxide-based Materials and Devices IV, International Society for Optics and Photonics, 2013, pp. 86261F.
[32] R.A. El-Mallawany, Tellurite glasses handbook: physical properties and data, CRC press 2016.
[33] H. Sun, C. Yu, G. Zhou, M. Liao, Z. Duan, L. Hu, J. Zhang, Comparative investigation of up-conversion luminescence in Tm^{3+}/Yb^{3+}-codoped germanate–niobic and germanium–bismuth glasses: effect of phonon density on up-conversion emission, Solid state communications, 134 (2005) 721-724.
[34] H. Sun, C. Yu, Z. Duan, L. Wen, J. Zhang, L. Hu, S. Dai, Optical transitions of Er^{3+} and Yb^{3+} ions in novel oxyfluoride bismuth–germanium glass: Observation of up-conversion, Optical Materials, 28 (2006) 448-452.
[35] D. Shi, Y. Zhao, X. Wang, J. Liu, Effects of Bi_2O_3 on up-conversion luminescence properties of Tm^{3+}/Yb^{3+}-codoped Ga_2O_3-GeO_2-Bi_2O_3-PbO glass, Physics Procedia, 48 (2013) 172-178.
[36] Y. Liu, D. Chen, Q. Zhang, Z. Jiang, Frequency up-conversion properties of Er^{3+}-doped TeO_2–ZnO–$PbCl_2$ oxyhalide tellurite glasses, Optical Materials, 28 (2006) 302-305.
[37] B. Dubois, H. Aomi, J. Videau, J. Portier, P. Hagenmuller, New oxyhalide glasses involving Sb_2O_3, Materials research bulletin, 19 (1984) 1317-1323.

[38] B. Dubois, J. Videau, M. Couzi, J. Portier, Structural approach of the ($xPbCl_2$−(1− x) Sb_2O_3) glass system, Journal of non-crystalline solids, 88 (1986) 355-365.
[39] G. Poirier, M. Poulain, M. Poulain, Copper and lead halogeno-antimoniate glasses, Journal of non-crystalline solids, 284 (2001) 117-122.
[40] B. Raghavaiah, N. Veeraiah, The role of As_2O_3 on the stability and some physical properties of PbO–Sb_2O_3 glasses, Journal of Physics and Chemistry of Solids, 65 (2004) 1153-1164.
[41] M. Legouera, P. Kostka, M. Poulain, Glass formation in the Sb_2O_3–$ZnBr_2$ binary system, Journal of Physics and Chemistry of Solids, 65 (2004) 901-906.
[42] M. Soltani, T. Djouama, A. Boutarfaia, M. Poulain, New heavy metal oxide glasses based on Sb_2O_3, J. Optoelectron. Adv. Mater. Symp, 2009, pp. 339-342.
[43] Y. Taibi, M. Poulain, R. Lebullenger, L. Atoui, M. Legouera, Physical properties of new Sb_2O_3-V_2O_5-K_2O glasses, Journal of Optoelectronics and Advanced Materials, 11 (2009) 34.
[44] M. Iezid, M. Legouera, F. Goumeidane, M. Poulain, V. Nazabal, R. Lebullenger, Glass formation in the Sb_2O_3–$CdCl_2$–$SrCl_2$ ternary system, Journal of Non-Crystalline Solids, 357 (2011) 2984-2988.
[45] F. Goumeidane, M. Legouera, M. Iezid, M. Poulain, V. Nazabal, R. Lebullenger, Synthesis and physical properties of glasses in the Sb_2O_3–$PbCl_2$–MoO_3 system, Journal of Non-Crystalline Solids, 357 (2011) 3572-3577.
[46] T. Som, B. Karmakar, Infrared-to-red upconversion luminescence in samarium-doped antimony glasses, Journal of Luminescence, 128 (2008) 1989-1996.
[47] F.D. Bloss, An introduction to the methods of optical crystallography, Holt Rinehart and Winston1961.

[48] Goumeidane F, Iezid M, Melik B, Ouannes K, Legouera M, Poulain M, T. Satyanarayana, P. Syam Prasad, P. Venkateswara Rao, Influence of molybdenum oxide on structural, optical and physical properties of oxychloride glasses for nonlinear optical devices, Ceramics International, 43 (2017) 11305-11311.

[49] S. Xu, Z. Yang, G. Wang, S. Dai, J. Zhang, L. Hu, Z. Jiang, Optical transitions and upconversion mechanisms in Er^{3+}-doped heavy metal oxyfluoride germanate glass, Journal of alloys and compounds, 377 (2004) 253-258.

Figure 1: DSC curve of the 80 Sb_2O_3 – 10 $ZnBr_2$ – 10 KCl glass. It shows the vitreous transition and the crystallization peak. Heating rate 10 K/min.

Figure 2.a: UV-visible transmission curve of glass 80 Sb_2O_3 – 10 $ZnBr_2$ – 10 KCl. The cut off wavelength for a 3 mm thick sample is $\lambda_{CUT\text{-}OFF}$ = 417 nm.

Figure 2.b: Infrared transmission of an 80 Sb_2O_3 – 10 $ZnBr_2$ – 10 KCl glass sample, 3 mm in thickness. The transmission limit due to multiphonon absorption is λ_{MP} = 7.85 µm.

Figure 3: Up-conversion emission at room temperature of 80 Sb_2O_3 – 9.8 $ZnBr_2$ – 10 KCl – 0.2 NdF_3 glass doped with Nd^{3+}. Green light emission (536 nm): $^4G_{7/2} \rightarrow {}^4I_{9/2}$ under 805 nm excitation.

Figure 4: Up-conversion emission at room temperature of 80 Sb_2O_3 – 9.8 $ZnBr_2$ – 10 KCl – 0.2 SmF_3 glass doped with Sm^{3+}. Visible emission lines: green (536 nm); orange (600 nm) and red (631 nm and 645 nm) corresponding to the transitions: $^4G_{5/2} \rightarrow {}^6H_J$ (J=5/2; 7/2; 9/2; 11/2). Infrared excitation at 949 nm.

Figure 5: Up-conversion emission of the 80 Sb_2O_3 – 9.8 $ZnBr_2$ – 10 KCl – 0.2 ErF_3 glass. Measured at room temperature. Green light emission (531 nm): $^4S_{3/2} \rightarrow {}^4I_{15/2}$ under 798 nm infrared excitation.

Figure 6: Up-conversion emission of 80 Sb_2O_3 – 9.8 $ZnBr_2$ – 10 KCl – 0.1 Yb^{3+} – 0.1 ErF_3 glass. (Yb^{3+} / Er^{3+} co-doping). Room temperature measurements. Green emission at 524 nm ($^2H_{11/2} \rightarrow {}^4I_{15/2}$) and red emission at 543 nm ($^4S_{3/2} \rightarrow {}^4I_{15/2}$) and 650 nm: ($^4F_{9/2} \rightarrow {}^4I_{15/2}$) under IR excitation at 980 nm.

Figure 7: Energy diagram describing the up-conversion process of Nd^{3+} in 80 Sb_2O_3 – 9.8 $ZnBr_2$ – 10 KCl – 0.2 NdF_3 glass.

Figure 8: Energy diagram explaining the up-conversion process of Sm^{3+} in the 80 Sb_2O_3 – 9.8 $ZnBr_2$ – 10 KCl – 0.2 SmF_3 glass.

Figure 9: Energy diagram explaining the up-conversion process of Er^{3+} in the 80 Sb_2O_3 – 9.8 $ZnBr_2$ – 10 KCl – 0.2 ErF_3 glass.

Figure 10: Energy diagram accounting for the up-conversion process in the Yb^{3+}/Er^{3+} co-doped glass: 80 Sb_2O_3 – 9.8 $ZnBr_2$ – 10 KCl – 0.1 YbF_3 – 0.1 ErF_3.

Figures

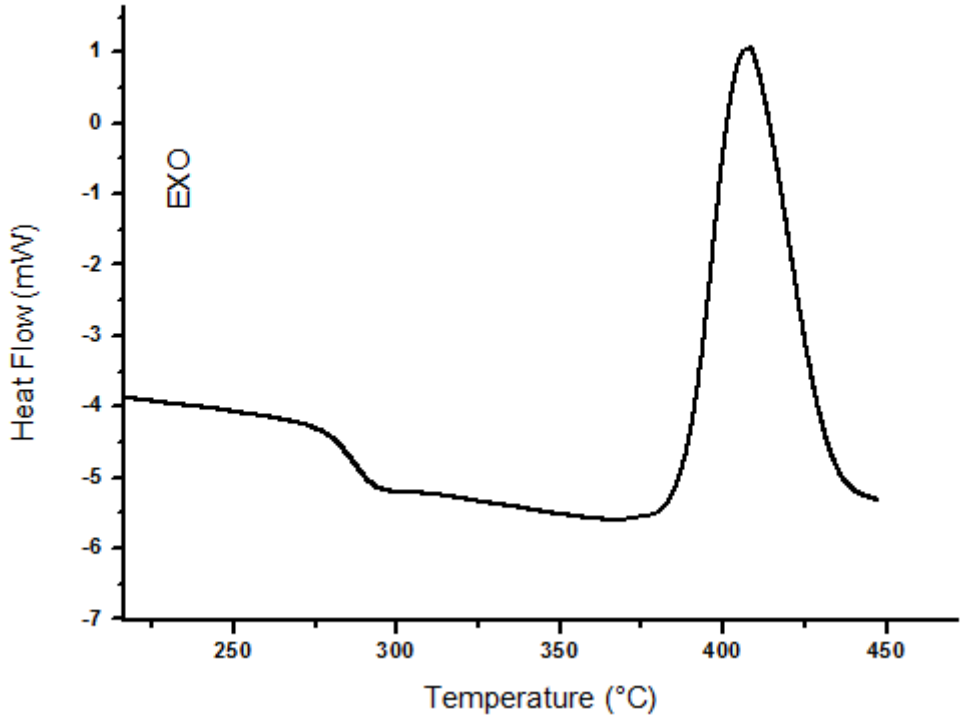

Figure 1

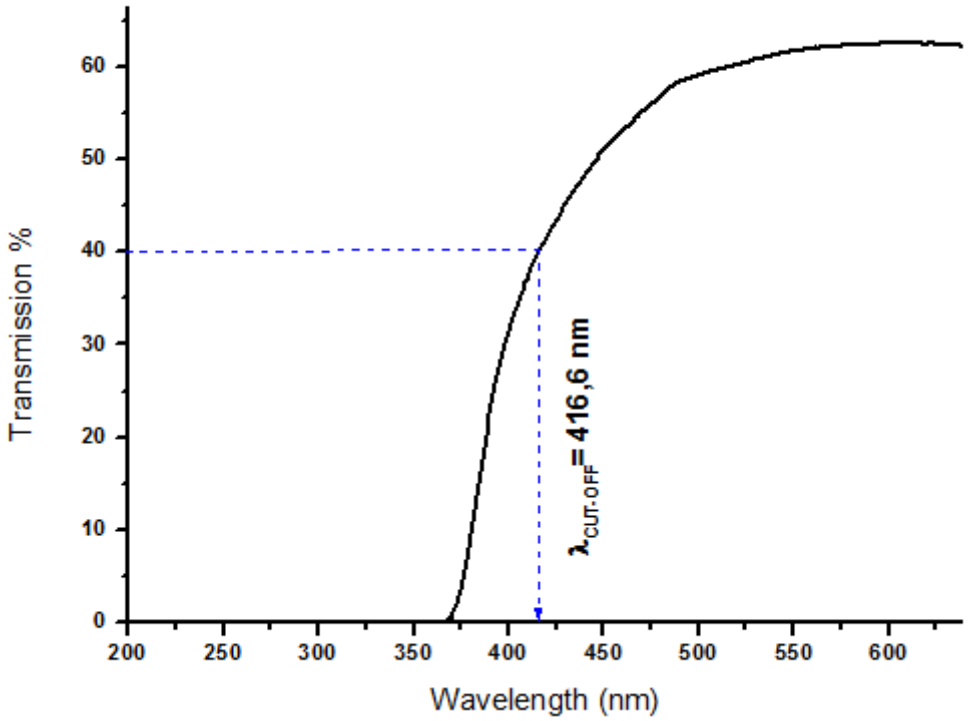

Figure 2.a

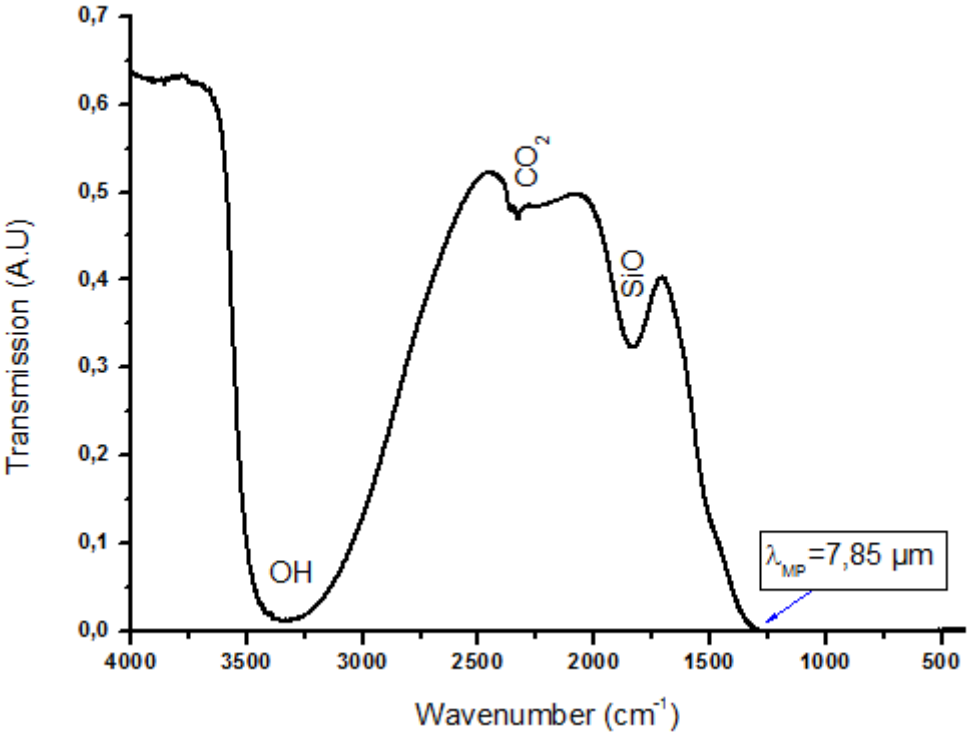

Figure 2.b

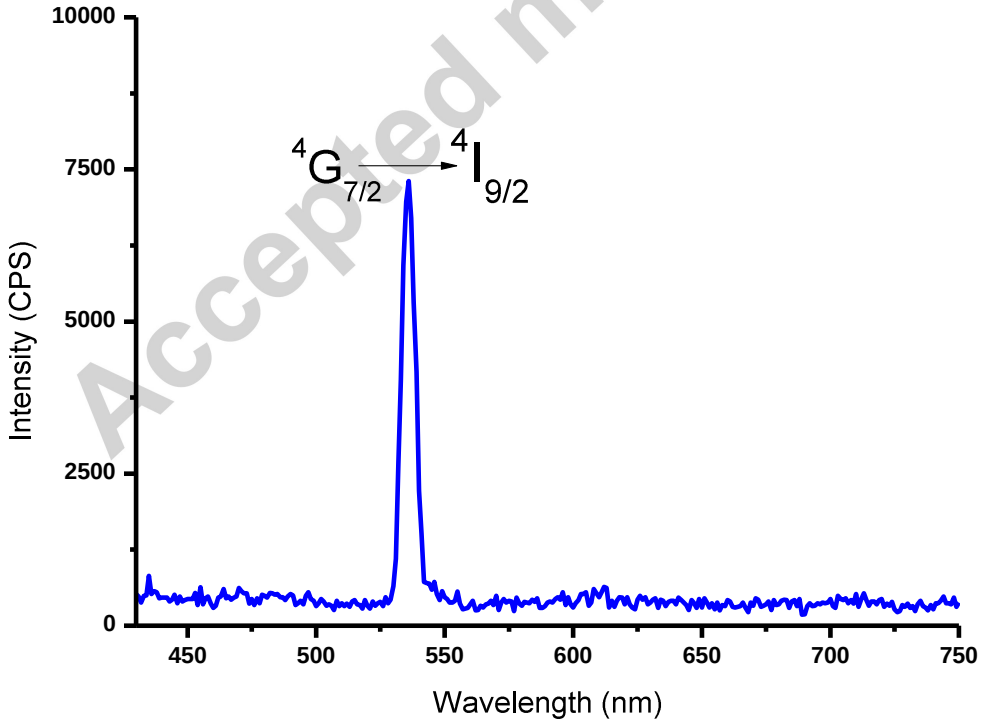

Figure 3

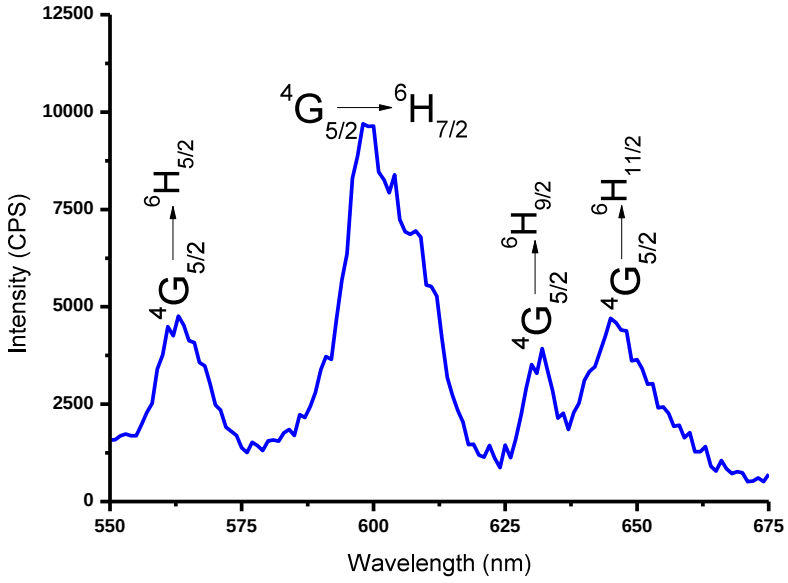

Figure 4

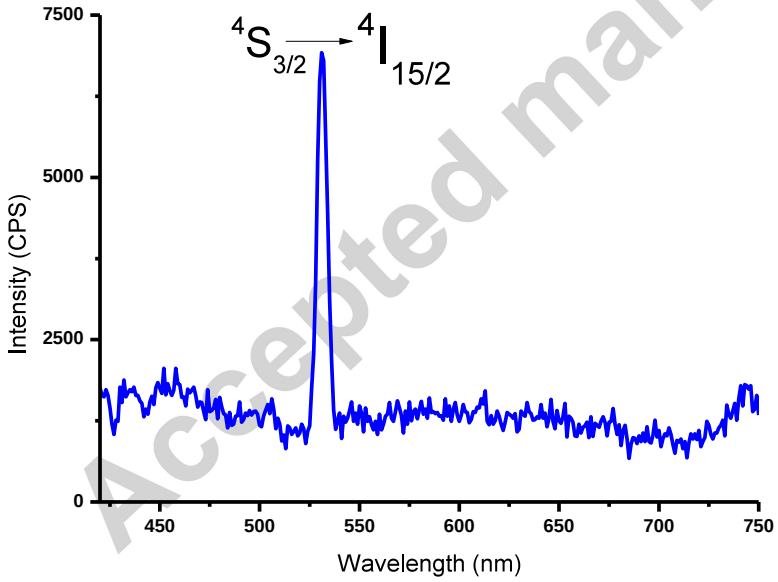

Figure 5

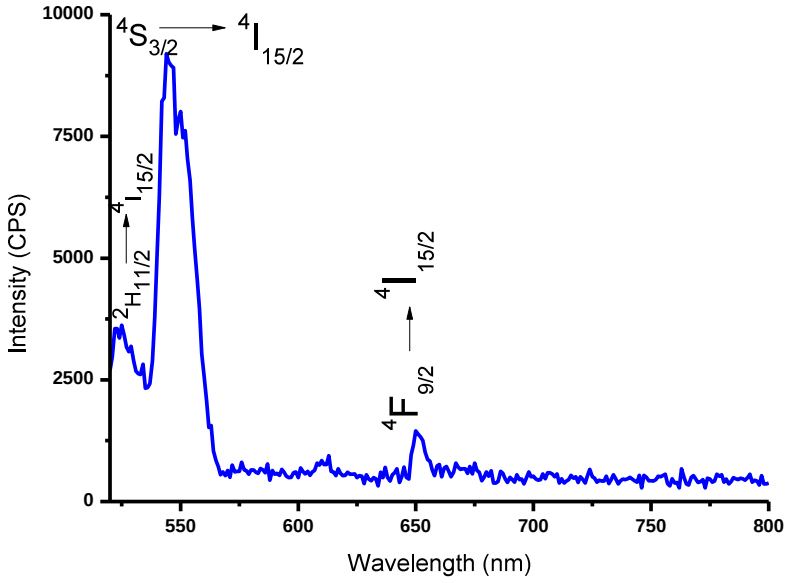

Figure 6

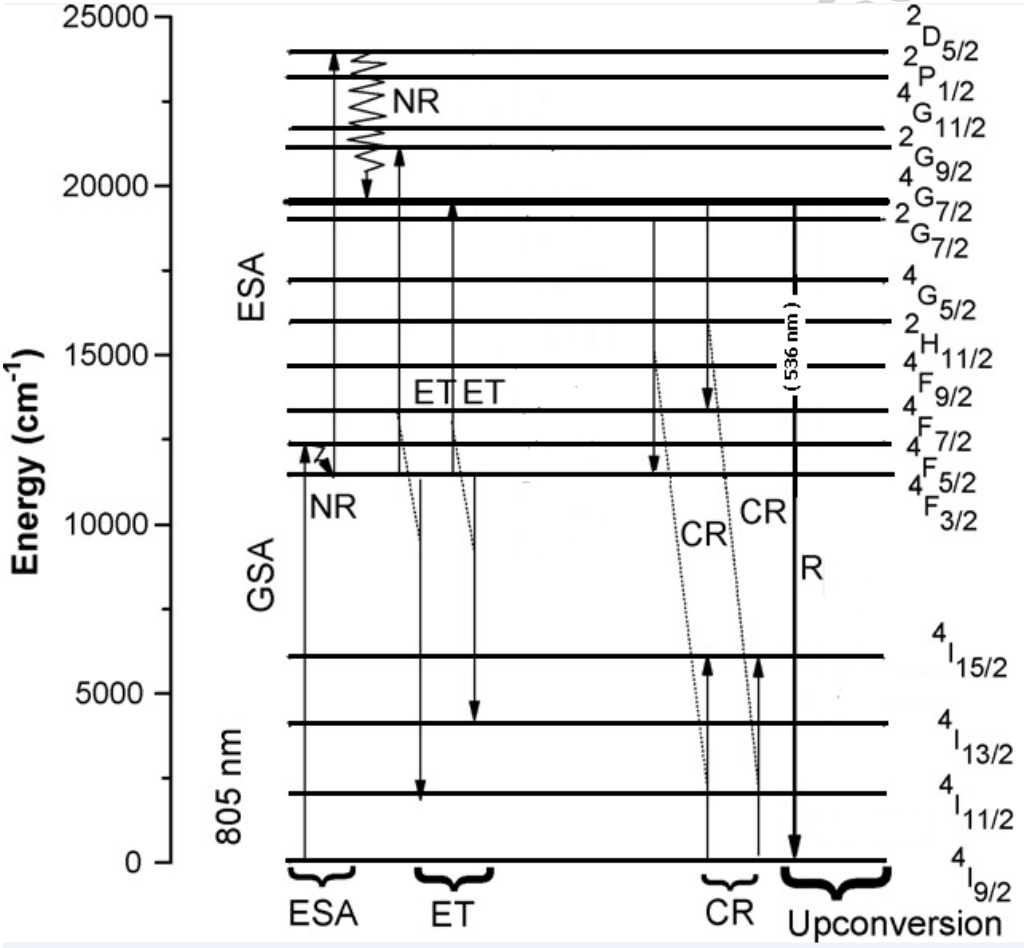

Figure 7

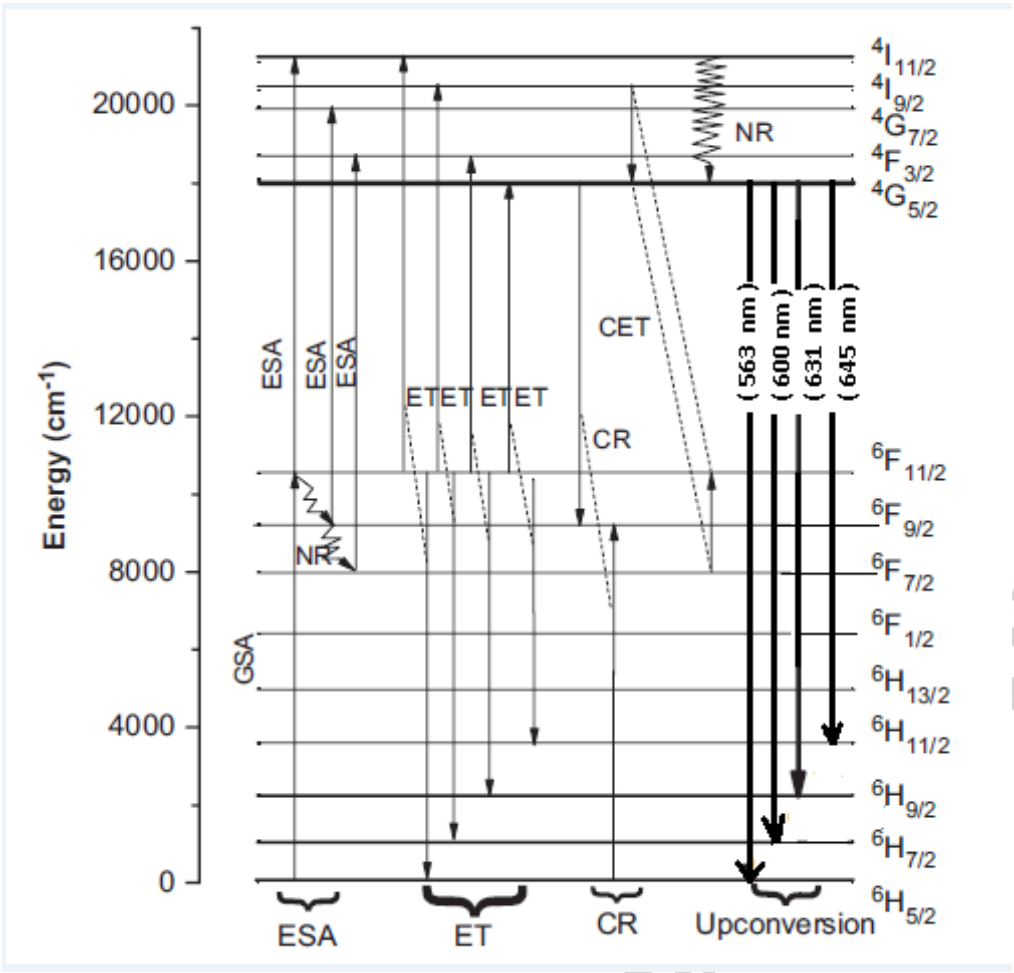

Figure 8

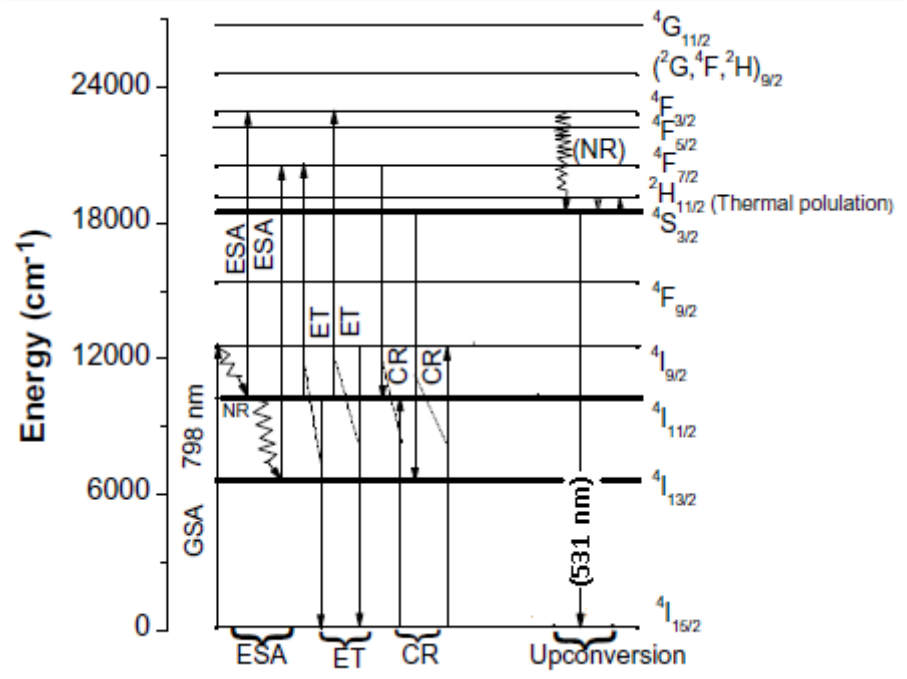

Figure 9

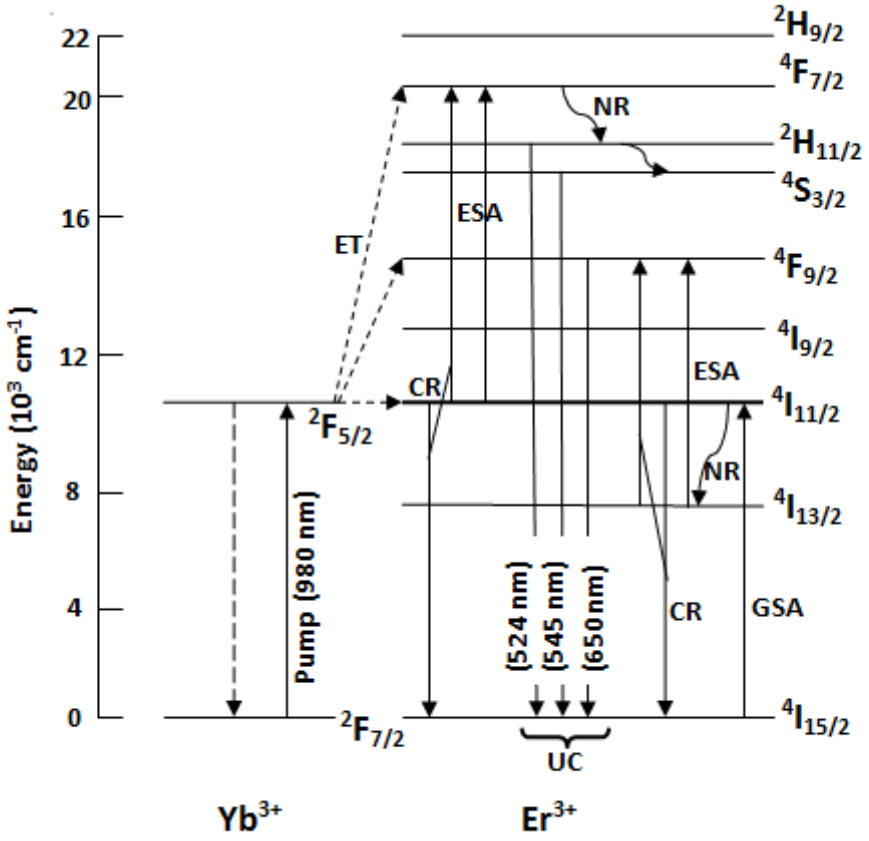

Figure 10

Tables

Density (g/cm^3)	Characteristic temperatures (°C)			CTE (K^{-1})
ρ±0.005	T_g ±2	T_x ±2	T_p ±1	(α ± 0.2)X10^{-6}
5.0831	275	384	407	19.5

Table 1a: The physical characteristics of the $80Sb_2O_3$–$10ZnBr_2$–10KCl glass: density, characteristic temperatures (T_g for glass transition;T_x for onset of crystallization;T_p for exotherm maximum) and Coefficient of Thermal Expansion (CTE).

Transmission Threshold UV-visible (nm)	Zero Transmission limit Infra-red (µm)	Refractive Index	Quantity OH (ppm)
$\lambda_{CUT\text{-}OFF}$ ±1	λ_{MP} ±0.025	n±0.01	Q
417	7.85	1.97	164

Table 1b: Optical characteristics of the 80 Sb_2O_3–10 $ZnBr_2$ –10 KCl glass: transmission thresholds in the UV-visible ($\lambda_{CUT\text{-}OFF}$) and infra-red spectrum (λ_{MP}); refractive index; (OH) concentration.